

**Review book title:
RECENT RESEARCH DEVELOPMENTS
IN ASTRONOMY & ASTROPHYSICS.**

**Dark and luminous matter connections.
Towards understanding galaxy evolution.**

Short title: Insights into galaxy evolution

Paola Mazzei

INAF, Astronomical Observatory, Padova
Vicolo dell' Osservatorio,5, 35122 Padova, Italy
e-mail: mazzei@pd.astro.it

ABSTRACT

In this review we outline the major points of *ab-initio* cosmological models focusing on some galaxy evolution unresolved problems. In particular our knowledge of the star formation rate which leads galaxy evolution, i.e. luminosity, colors and dust enrichment, is still very poor. Smoothed particle hydrodynamic simulations including chemo-photometric evolutionary population synthesis models of isolated collapsing systems endowed with triaxial dark matter halos, gas and the star formation switched on, are a useful tool to shed light on several open questions. This approach, which allows a greater particle resolution than a fully consistent cosmological scenario, gives us important insights into connections between dark and luminous matter. Both the initial properties of the halo, as so as its geometry and dynamical state, and total mass of the system, drive the galaxy formation and evolution. In our simple framework spiral galaxies arise only in systems with both a total mass less than $10^{12} m_{\odot}$ and a critical value of the baryonic-to-total-mass ratio, around its cosmological value, 0.1. For the same value of such a ratio more massive systems host more luminous and redder galaxies, as a consequence of the stronger burst of star formation arising into their halos earlier on. Moreover the star formation does not switch on in the less massive DM halos so that the critical mass to entail a luminous system is $\simeq 10^{11} m_{\odot}$. For a given total mass, higher values of the baryonic-to-total-mass ratio provide galaxies with lower rotational support so that no constraints to the total mass of the system hosting an elliptical galaxy have been derived.

1. INTRODUCTION

Studies of the large-scale distribution of galaxies point toward understanding fundamental hypotheses as so as the identity of the dark matter (DM), the nature of the initial density perturbations and the mechanism of structure growth. Although none of these issues can be regarded as settled, there is now a growing consensus that cold dark matter (CDM) is the most likely candidate for the DM, that cosmic structure grew by the gravitational amplification of random phase initial density fluctuations of inflationary origin, and that the fundamental cosmological parameters have the following values: density parameter, $\Omega_0 = 0.3$, cosmological constant term, $\Lambda_0 = 0.7$ and Hubble constant, H_0 which, in units of 100 km/s/Mpc, corresponds to $h = 0.7$. Cosmological constraints reflect only one aspect of the information encoded in the galaxy clustering. Another, equally interesting aspect, concerns the processes responsible for the formation and evolution of the galaxies. The past two

decades have witnessed the emergence of a successful class of *ab-initio* theoretical models to explain the formation of the structures in the Universe. The initial conditions consist of the cosmological parameters (Ω , Λ , H_0) and of an initial fluctuation spectrum such as the CDM power spectrum. The remaining parameter, i.e. the amplitude of these initial fluctuations, is calibrated by the measured anisotropies of the microwave background. Numerical simulations have become an important tool for exploring the detailed predictions of these *ab-initio* models. However, extending these studies to understand the formation of luminous components of galaxies is difficult since our knowledge of the star formation process and its interaction (feedback) with the surrounding interstellar medium is still rather limited. Moreover, computational resources strongly constrain their baryonic resolution, thus most of the simulations that focused on the formation of individual galaxies were not performed in a cosmological scenario [1, 2, 3, 4, 5, 6]. In this framework [4, 6] (therein after we will refer to these papers as to paper I and II respectively) were the first to present results from smoothed particle hydrodynamic (SPH) simulations of isolated collapsing triaxial systems, initially composed of DM and gas, implemented with chemo-photometric evolutionary population synthesis (EPS) models providing the Spectral Energy Distribution (SED) from UV up to near-IR K band.

In this review we will outline the major challenges of *ab-initio* models and our efforts to emphasize connections between dark and luminous matter. The plan of this paper is the following: the next section briefly reviews the major points of these class of *ab-initio* models. Section 3 focuses on galaxy formation in a hierarchical scenario and on its major problems. Section 4 presents our approach and points out results from paper I and II concerning galaxy formation and evolution in a simple framework, the monolithic scenario. We will discuss the star formation rate (SFR) and the rotational support (i.e. the ratio between rotational to kinetic energy) of the baryons (gas+stars) provided by these simulations and derive some issue concerning galaxy morphological types and their dependence on the properties of the whole system in particular of their DM halo. Important findings, summarized in Section 5, are that the total mass of the system, the DM halo initial geometry, given by different values of initial triaxiality ratio and its dynamical state, strongly reflect on galaxy formation and evolution. Moreover we outline the role of different values of the baryonic to total mass ratio, M_{bar}/M_{tot} showing that its cosmological value, around 0.1, coupled with the less massive halos ($M_{tot} \leq 10^{12} m_{\odot}$), strongly favors formation of disk galaxies as obtained in a fully consistent cosmological scenario [7] where disks are the first galaxy outcome.

2. NUMERICAL SIMULATIONS OF HIERARCHICAL CLUSTERING

During the last decade, significant progress has been made in understanding cosmic structure formation and evolution. Structure grows as objects of progressively larger mass merge and collapse to produce new virialized systems. The formation of dark halos in different cosmologies has been studied in detail with high resolution simulations [8, 9, 10, 11] to determine the large-scale mass distribution, the halo merging histories, the structural parameters of the DM halos and finally the formation of galaxies inside these halos. In many respects, these simulations are in agreement with observations, for example, with the present day abundance of massive galaxy clusters, the shape and amplitude of galaxy clustering patterns, the magnitude of large scale coherent motions of galaxy systems, among the others [12]. However several difficulties still remain. Firstly, the universal cuspy density profiles of DM halos [9, 13, 14] while agree with observations of galaxy clusters are in disagreement with flat density DM distributions inferred from observations in the centers of galaxies [15, 16, 17]. As outlined by [12], halos formed in a Λ CDM scenario are too centrally concentrated to be consistent with observations of the dynamic of our own Galaxy. Moreover the actual physical mechanisms responsible for such an universal density profile are as of yet not well understood. [18] argue that the universal profile does not depend crucially on hierarchical merging but this is a more generic feature of the gravitational collapse in an expanding universe which produces a near universal angular momentum distribution among the halo particles. However the same result is derived from SPH simulations of isolated collapsing triaxial systems ([4], paper I). [4] indeed argue that such a profile is a consequence of violent relaxation which erases all information related with the initial configuration, thus also any cosmological signature.

Secondly, [13] and [19] demonstrated that CDM scenario predicts that the local group should have fifty times as many dwarf galaxies than actually observed. In order to reconcile predictions with observations a spectrum would be required that suppresses power on galactic and subgalactic scales while keeping the large scale properties of the model virtually unchanged. This would in principle allow galaxy-sized halos to collapse later and thus become less centrally concentrated. However in such a case, they may hinder the formation of massive galaxies at high redshift, at odds with the mounting evidence that such galaxies are fairly common at $z \geq 3$ [20].

Thirdly, the specific angular momentum and the scale length of the disk galaxies in the cosmological simulations are too small compared to real galaxies [21]. This may be partially a numerical problem of SPH simulations (see Section 3), but it is more likely due to very efficient cooling and angular momentum transport from the baryons to the dark halos during merger events.

Forthly, in a hierarchical scenario it is very difficult to fit properties of SCUBA sources

detected, from sub-millimetric surveys, at high redshift ($z > 2$) and requiring very high star formation rates ($\gg 100 m_{\odot}/yr$) [22, 23]. In particular their number density is under-predicted also by semi-analytical models [24]. These *ab-initio* models are based on numerical simulations as far as dissipationless physics is concerned however encode the dynamics of cooling gas, star formation, feedback and galaxy mergers into few simple rules which allow the process of star formation within DM halos to be calculated [25, 26, 27]. The same models fail to reproduce the large number of high- z galaxies detected in K-band surveys with both Extremely Red Colors (EROs) $R - K > 5$, $K \simeq 17 - 22$, [28, 29] and spectrophotometric properties consistent with old stellar populations up to $z \simeq 1.5$ [30, 31].

3. GALAXY FORMATION AND EVOLUTION

Following the pioneering work of [32], one of the critical processes during galaxy formation is the radiative cooling. All the gas in virialized systems cool at their center in a runaway process (over-cooling) which can be halted if a) a large fraction is transformed into stars, b) most of the gas settles in a rotationally supported disc, or c) some energy input reheat the gas [33]. As we will discuss with more details later on (Section 4.1.2), since our understanding of the star formation (SF) process and its interaction with the surrounding interstellar medium (feedback) is still rather limited, simulations including such a process are based on phenomenological approaches. [34] have analyzed the effect of different SF recipes in N-body/SPH cosmological simulations of galaxy formation. Even if their simulations achieve very poor galaxy resolution (more than 32 particles), nevertheless these provide interesting results by comparing different runs. They conclude that results do not depend strongly on different SFR prescriptions when feedback is neglected: the ratio of cold gas to stars in the final galaxy is primarily controlled by the range of gas density where the SF is allowed to proceed efficiently. However the fraction of gas that cools is always much too high to account for the K-band luminosity function so that feedback must be accounted for. Therefore, once stars are present they are expected to return to the interstellar medium (ISM) part of their mass and energy via supernovae (SNe) explosions, stellar winds and ultraviolet (UV) flux. These latter contributions are relevant only for massive stars. All this is known as the stellar energy feedback. There are two ways of including phenomenological feedback models from type II supernova energy in cosmological simulations: thermal and kinetic. In the former case all the energy (from SNe, stellar winds and UV flux) supplies the thermal budget of neighboring gas particles [35, 36], in the second one only a fraction of this energy is allowed kinetically to affect the surrounding particles. This fraction is a free parameter [37, 38]. However thermal feedback can reduce the SFR appreciably only if the reheated gas is prevented from cooling for a considerable fraction of the Hubble time.

Indeed most of the stars form in high density regions where the thermal energy can be lost to radiation very quickly. Dumping the SNe energy as velocity perturbations does affect the SFR, because it can halt or reverse the local collapse of a region. Therefore feedback inclusion is a very critical point for such simulations.

Computational resources strongly constrain the baryonic resolution of numerical simulations, thus most of the simulations that focused on the formation of individual galaxies were not performed in a fully cosmological scenario [1, 2, 3, 4, 5, 39, 6], (see also Section 4). [7] present the first results of simulations including SF and feedback to focus on the origin of galaxy morphologies in a CDM Universe. Their claim for sufficiently high gas particle resolution to allow for such a study. Their findings are that Hubble sequence reflects different accretion histories in the hierarchical framework. Disks arise from the smooth deposition of cooled gas at the center of DM halos, spheroids from the stirring of preexisting disks during mergers. Thus galaxy morphology is a transient phenomenon within the lifetime of the galaxy. The first attempts to analyze with greater detail formation and evolution of a single disk galaxy inside cosmological scenario have been performed very recently [40, 41]. The general problem affecting disk galaxies in a hierarchical Universe is their higher concentration than observed in spiral galaxies. This is a consequence of the formation process of the disks. During the mergers needed to assemble their mass, the gas component, owing to dynamical friction, transfers most of its angular momentum to the surrounding halos. Simulations show that while the specific angular momentum of the DM increases with decreasing redshift, that of gaseous disk decreases. So the spin of the disks is about one order of magnitude lower than expected for spiral galaxies and the disk scale length is shorter than observed. This produces an offset in the I-band Tully-Fisher (TF) relation. Its slope and scatter (lower than the observed $\simeq 0.4 \text{ mag}$) are fairly in good agreement with the observations but its zero-point is in serious disagreement with the data. The simulated TF relation is almost two magnitudes faint at a given rotation velocity (see Fig. 1 from [12]).

Recent attempts to translate in photometric information the results of disk evolution in a cosmological scenario [41] derive a bulge-to-disk ratio 1:1 in the total (integrated) light. The final system ($z=0$) rotates faster and appears more concentrated than observed for its mass living 1 mag off the I-band TF relation.

4. ISOLATED COLLAPSING TRIAXIAL SYSTEMS

[4] were the first to present results from SPH simulations of isolated collapsing triaxial systems, initially composed of DM and gas, implemented with chemo-photometric evolutionary population synthesis (EPS) models providing the spectral energy distribution (SED)

from UV up to near-IR K band. They have focused on the final properties of the systems, i.e. after 15 Gyr in the rest-frame, for different values of the stellar initial mass function (IMF) parameters (i.e.: $\phi(m) \propto m^{-\alpha}$ where α is slope and m_{low} its lower mass limit) and feedback strength self-consistently accounted for (see Section 4.2.2). In paper II, [6] have deepened the analysis focusing on the time behavior of the SFR and on the rotational support achieved by their luminous systems. The initial configuration is the same in both the papers however in paper II higher particle resolution runs have been performed and a wider range of initial conditions of the collapsing systems have been analyzed (Table 1). They aimed to shed light into the dependence of the system evolution on some parameters completely unexplored such as the total mass, initial geometry and dynamical state of the DM halo. Moreover also the effects of different values of the baryonic-to-total-mass ratio (0.1 their fiducial value) have been investigated. They found important connections between dark and luminous matter.

4.1. Recipes

4.1.1. *The initial configuration*

As described in paper I, the system is built up with a density distribution i) $\rho \propto r^{-1}$, ii) a spin parameter, λ [42] given by $|\mathbf{J}||E|^{0.5}/(GM^{0.5})$, where M is the total mass, E the total energy, J the total angular momentum and G the gravitational constant, equal to 0.06 and aligned with the shorter principal axis of the DM halo, and iii) a triaxiality ratio of the DM halo as detached by the Hubble flow in a CDM scenario, $\tau = (a^2 - b^2)/(a^2 - c^2)$ [43] where $a > b > c$, equal to 0.58. The effect of a different initial geometry, i.e. of a slightly oblate ($\tau=0.45$) and of a prolate ($\tau=0.84$) halo, has been investigated. Different λ values are also considered to give insight into the role of the dynamical state of the halo on the evolution of the baryonic matter. All the simulated systems have the same initial virial ratio, 0.1, and the same average density to avoid a different collapse time. The total initial number of particles ranges between 2000 to 20000 with $N_{DM} = N_{gas}$. The system evolves up to 15 Gyr in the rest-frame; the final number of particles ranges from 10000 to 200000.

All the simulations performed in papers I and II include self-gravity of gas, stars and DM, radiative cooling, hydrodynamical pressure, shock heating, artificial viscosity, SF and feedback from evolved stars and type II SNe.

4.1.2. *The star formation rate*

As described in Section 3, the phenomenological approach for such a process translates in a power law dependence of the SFR on the local gas density. In all the cases the basic procedure is the same: at the end of each time step, a subset of gas particles is being identified as eligible to form stars. A fraction of them are then converted into stars which are subsequently subject only to gravitational interactions.

The star forming criterion adopted in paper I and II is based on following conditions [37]: i) the local gas density must be larger than a threshold value, $7 \times 10^{-26} \text{ gr/cm}^3$, which corresponds to the Jeans instability criterion and to cooling time shorter than dynamical time in the region, and ii) the gas particle must be in a convergent flux, i.e. $\Delta v < 0$, so pressure forces are unable to stop the collapse. A gas particle satisfying these conditions loses a fraction ϵ of its mass which becomes a star particle; $\epsilon=0.4$ is the fiducial value however the effect of different choices have been also examined (0.2 in paper I and 0.04 in paper II) to account for the impact of this parameter too on the results.

4.1.3. *Feedback strength and initial mass function*

The feedback effects are both thermal and kinetic as described above (Sect. 3). A fraction f_v of SNe energy is supplied to neighboring gas particles in the form of kinetic energy, with the rest, $(1 - f_v)$, being added as heat. Paper II assumes $f_v = 0.01$ as fiducial value. The kinetic energy implementation, due to the number of massive stars which are exploding as SNe during each time step per stellar generation, $\Delta N_*(m > 8 m_\odot)$, is given by: $\Delta E_{SNe,vel}[\text{erg/gr}] = f_v \eta$ where $\eta \simeq 5 \times 10^{17} \Delta N_*(m > 8 m_\odot)/M_*$ and M_* is the mass of a stellar generation which corresponds to a star particle. The value of the ratio $\Delta N_*(m > 8 m_\odot)/M_*$ depends on the IMF's parameters. As presented in paper I, B1 simulations correspond to $\alpha = 2.5$, $m_{low} = 0.1 m_\odot$ and $m_{up} = 100 m_\odot$ [44], B2 to $\alpha = 2.35$ with the same mass limits, B3 models to B2's parameters but with lower mass limit $0.01 m_\odot$ [45]. Given this self-consistent approach to account for feedback, B1 models provide a feedback strength 33% higher than B3, whereas B2 models 37% higher than B1 and 58% higher than B3 models.

4.2. Results

4.2.1. The SFR and the rotational support of the baryonic system

[6] find that, for a given value of the baryonic-to-total-mass ratio, the total mass of the system, M_{tot} ($10^{10} m_{\odot}$, in our units), controls the SFR. Fig.1 shows that in systems with larger M_{tot} the SF onset arises earlier on and the SFR achieves higher values than in the less massive halos. In the same figure the effect of a different IMF is also shown. B3 models allow higher SFR as a consequence of their lower feedback strength. Numerical resolution slightly affects the SFR, the other parameters being the same (Fig.2). Simulations providing only thermal feedback implementation (i.e. $f_v = 0$) provide a stronger burst of SFR which, as in the case of simulation in Fig.2 (panel ii) produces a residual gas fraction lower of about 24% (see also Table 2, col. 9). Fig.3 (panels a, b) compares the evolution of the rotational support of the baryons for some simulation in Fig.1 and Fig.2. We can see that the feedback strength, which depends on the total mass of the system through the SFR and the IMF's parameters, strongly affects the dynamical evolution of the luminous matter. This is because the lower the SFR the larger the fraction of cold ($T < 10^5 K$) rotating gas and the lower the amount of random motions induced by the kinetic feedback.

The rotational support of the baryons increases by rising resolution allowing the value expected for local Spirals (the maximum disk assumption requires that such a support is $\geq 85\% \pm 10\%$ of the total energy budget [49]) for a resolution of 6000 initial total particles.

Moreover even if the SFR, and thus the fraction of residual gas, are slightly depending on particle resolution, the fraction of cold gas is decreased of about 10% by reducing gas resolution from 3000 to 1000 particles. This is a very important point: a low resolution could strongly affect the results of cosmological simulations of galaxy formation provided by such a kind of feedback. The so called "angular momentum crisis", which together with over-cooling problem are some of the major challenges of cosmological simulations, could be solved accounting for both feedback and high particle galaxy resolution. Recent findings [40] point toward the same conclusion. Accounting for results of paper II (Fig.1), a suitable choice of IMF's parameters (B3 models) improve further this point. Moreover, as shown in Fig.3a, massive baryon systems achieve lower rotational support than the less massive ones. In summary, with the fiducial value of the M_{bar}/M_{tot} ratio, accounting for the dependence of the feedback strength on the IMF's parameters claimed above, B3 simulations with $M_{tot} \leq 10^{12} m_{\odot}$ are most suitable to match general properties of Spirals whereas more massive systems are required to match those of Ellipticals with the same IMF.

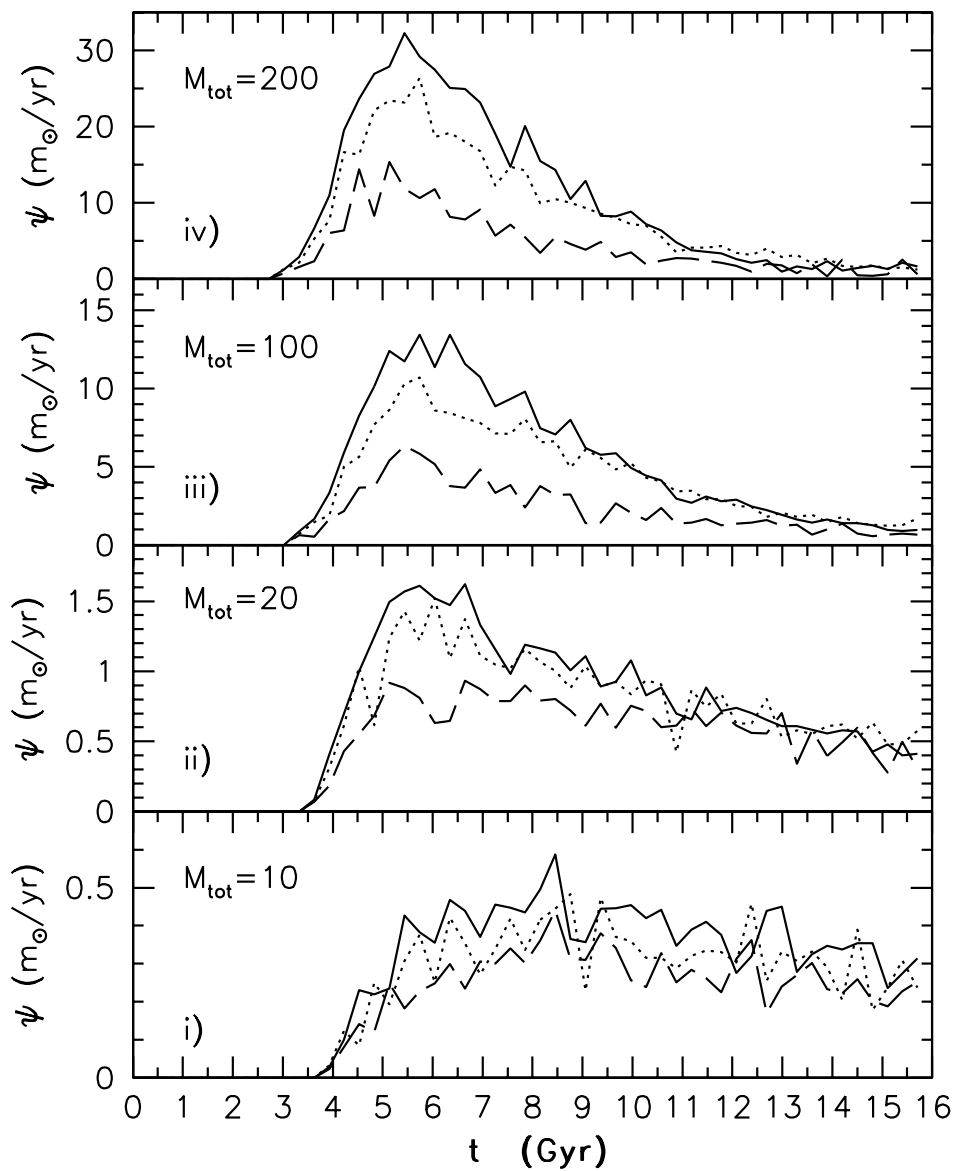


Fig. 1.— Time behavior of the SFR for runs with 6000 total initial particles, M_{bar}/M_{tot} ratio equal to 0.1, but different M_{tot} and different IMF's parameters (see text): B1 models, dotted line, B2 models, long dashed line, B3 models, continuous line.

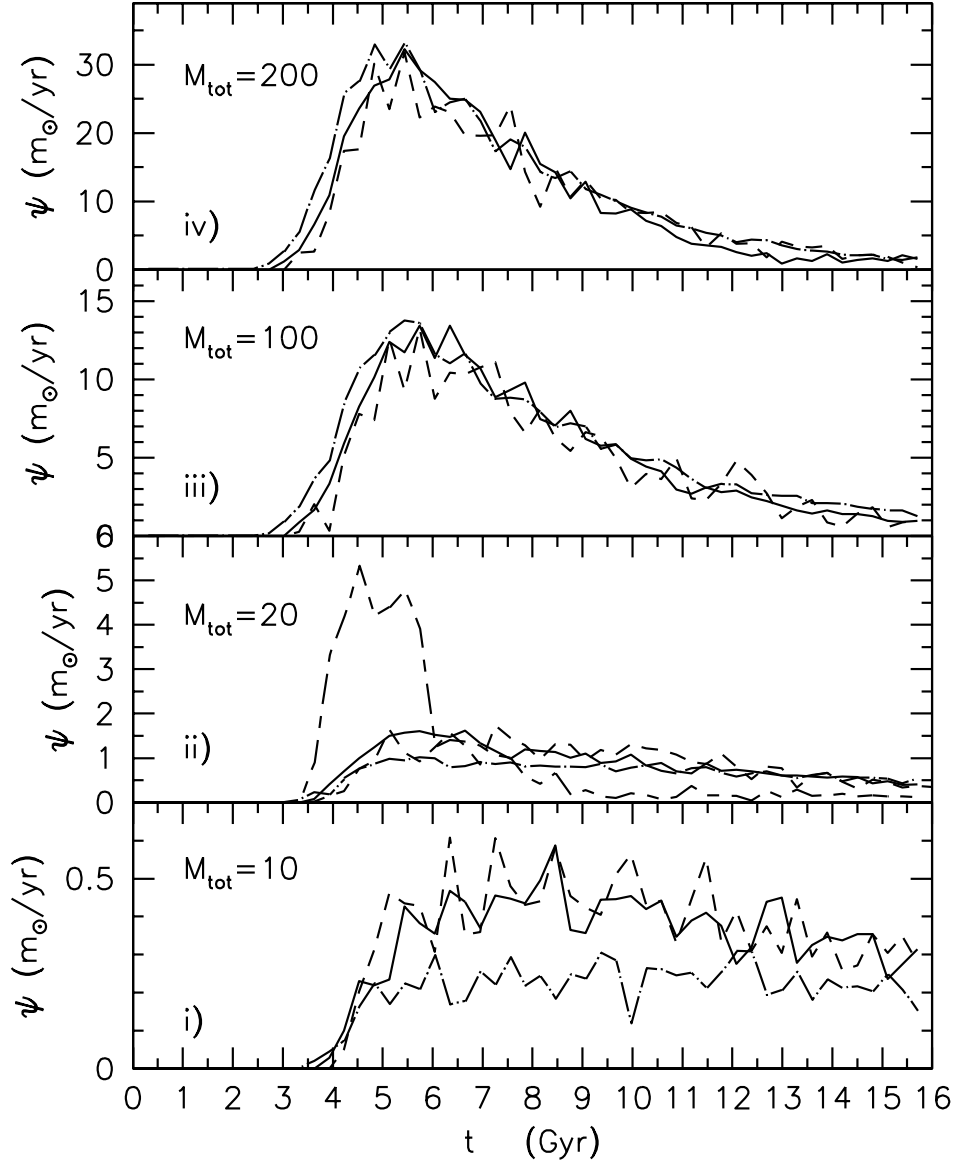


Fig. 2.— As in the previous figure for B3 models with different total initial particles: 6000, continuous line, 2000, short-dashed line and 20000, dot-dashed line; in panel ii) a run with only thermal feedback, i.e. $f_v = 0$ (see text), and 6000 total initial particles is also shown (long-short dashed line)

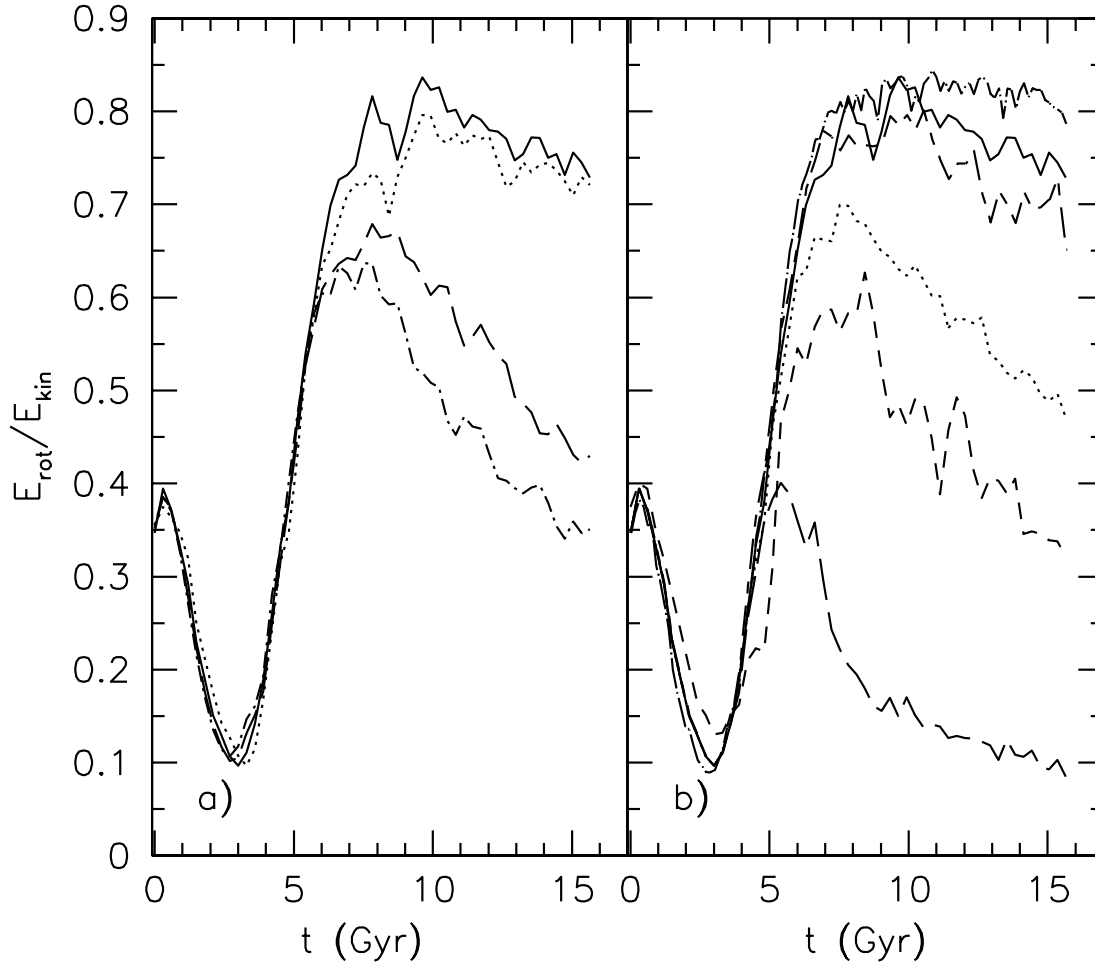


Fig. 3.— Right panel (a) compares the evolution of the rotational support of B3 models in Fig.1: $M_{tot}=10$ dotted line, $M_{tot}=20$ continuous line, $M_{tot}=100$ dashed line, $M_{tot}=200$ dot-dashed line; left panel (b) shows the same for models of panels ii) in Fig.1 and Fig.2 with the same symbols.

4.2.2. *The gas mass resolution*

The rise of the SFR with M_{tot} cited above, has been further investigated since by keeping constant the number of initial particles and the M_{bar}/M_{tot} ratio, more massive systems entail more massive gas clouds, so rising the mass of each gas cloud turned into stars for a given efficiency of SF, ϵ (see Section 4.1.2). Thus in paper II we performed several simulations by changing M_{tot} but keeping constant M_{bar} with the aim to resolve always the same mass of gas. The gas mass resolution ranges from $3.33 \times 10^6 m_{\odot}$ to $6.67 \times 10^7 m_{\odot}$; the lower resolution is better than that achieved both by [7], i.e. $1.27 \times 10^7 m_{\odot}$, and like that of [41], i.e. $3.29 \times 10^6 m_{\odot}$. Results concerning B3 simulations with $M_{bar} = 1$, gas resolution $3.33 \times 10^6 m_{\odot}$ and 6000 total initial particles, are shown in Fig. 4. The SFR depends on the DM mass, in the sense that it turns on later the larger M_{DM} even if the total mass of gas turned into stars is only slightly depending on M_{DM} value.

Looking at the dynamical evolution of the baryons, Fig. 5 shows that the fiducial M_{bar}/M_{tot} ratio (0.1) entails the largest rotational support. The growth of DM mass, which reduces this ratio well below its fiducial value, also reduces the rotational support of the baryons inside the system. Thus the rotational support of the simulated galaxy is strongly dependent also on the value of the M_{bar}/M_{tot} ratio.

To conclude such a check, some simulations have been performed with the same M_{bar}/M_{tot} ratio (0.1) but different total masses and ϵ values so that the same mass of each gas cloud turns on in a star particle. Thus a simulation with M_{tot} equal to 200 and ϵ equal to 0.04 has to be compared with one having $M_{tot} = 20$ and $\epsilon = 0.4$ (see Fig.5 in paper II). [6] derive that gas mass resolution does not affect the results strongly. For a given M_{tot} , the SFR does not depend on such a resolution neither on the efficiency of SF but it is driven by the initial amount of gas. Systems initially gas depleted show both longer delays of the SF onset, given the lower gas density achieved by the collapsing system, and lower SFRs.

The SF does not switch on in the less massive baryonic systems so that, for the fiducial value of the M_{bar}/M_{tot} ratio, the critical initial mass of gas to entail a luminous system is $\simeq 10^{10} m_{\odot}$.

4.2.3. *The initial geometry and dynamical state of the DM halo*

A new interesting point emphasized by these simulations is that galaxy formation and evolution is strongly affected by the initial geometry of the DM halo. For a given M_{tot} and M_{bar}/M_{tot} ratio, the lower τ the higher the SFR (Fig. 6a). This means that less favorable conditions to the SFR occur inside prolate halos ($\tau > 0.66$), the other parameters being the same. Moreover also the rotational support of the galaxy depends on this parameter

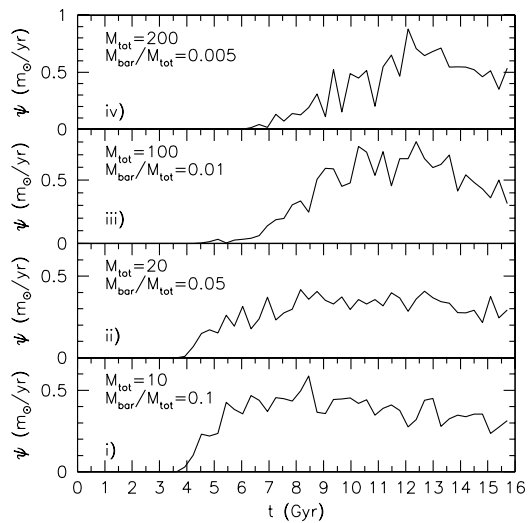


Fig. 4.— Time behavior of the SFR for B3 models with different M_{tot} but the same gas mass resolution (see text).

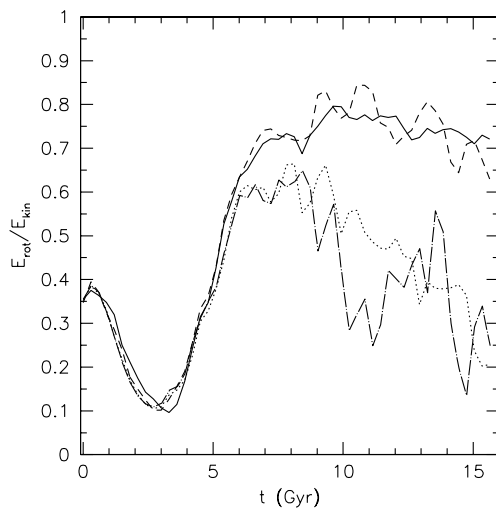


Fig. 5.— Time behavior of the rotational support of B3 models in Fig.4: $M_{tot}=10$ continuous line, $M_{tot}=20$ dashed line, $M_{tot}=100$ dotted line and $M_{tot}=200$ dotted-long dashed line.

(Fig.6b). So unfavorable conditions to spiral galaxy formation arise inside prolate halos. All the simulations discussed so far have been built up with initial spin parameter, λ , equal to 0.06 (Section 4.1.1). Simulations performed with different λ values, to give insight into the effects of a different initial dynamical state on the system evolution, show that the SF turns on later in systems with higher λ and such systems host galaxies endowed with lower rotational support (Fig.7a and Fig.7b respectively). Therefore inside strongly rotating halos spiral galaxy formation can be suppressed.

4.2.4. Chemo-photometric integrated properties

Photometric integrated galaxy properties depend on the SFR, for a given IMF choice [46, 47, 48]. Thus such properties are not affected by different particle resolution given the slight dependence of the SFR on such a resolution, outlined above. Integrated colors, luminosities, metallicities, together with mass-to-light ratios, disk scale lengths and so on, at 15 Gyr in the rest-frame, of simulations performed in paper I are presented in Tables 3, 4, 5, and 6 and in Fig. 17 of that paper. Given the wider range of parameters explored in paper II (Table 1), Fig. 8 shows colors and metallicities of all the simulated galaxies. Results are fully consistent with observations of local galaxies of different morphological types. More massive systems show redder colors, higher luminosity and mass-to-light ratios, moreover they are characterized by older stellar populations and higher stellar metallicities than the less massive ones. Furthermore the more massive simulated galaxies have lower residual gas fraction, and in particular less cold gas, than the less massive ones, in agreement with results of fully consistent cosmological simulations with very low galaxy-particle resolution [34].

Fig.9 compares the observed B-band TF relation [54] with predictions of simulations in Table 1. Table 2 summarizes disk-scale lengths and *bulge/disk* ratios derived for models in Fig.2b (panel ii). For an exponential disk we expect $r_{otp} = 3.2r_D$ [54], in agreement with findings in Table 2.

As we will discuss in the next section, results summarized here and in the previous Sections (4.2.1-4.2.3), translate in important issues concerning morphological galaxy types, in particular spiral galaxies, into the very simple framework of monolithic collapse.

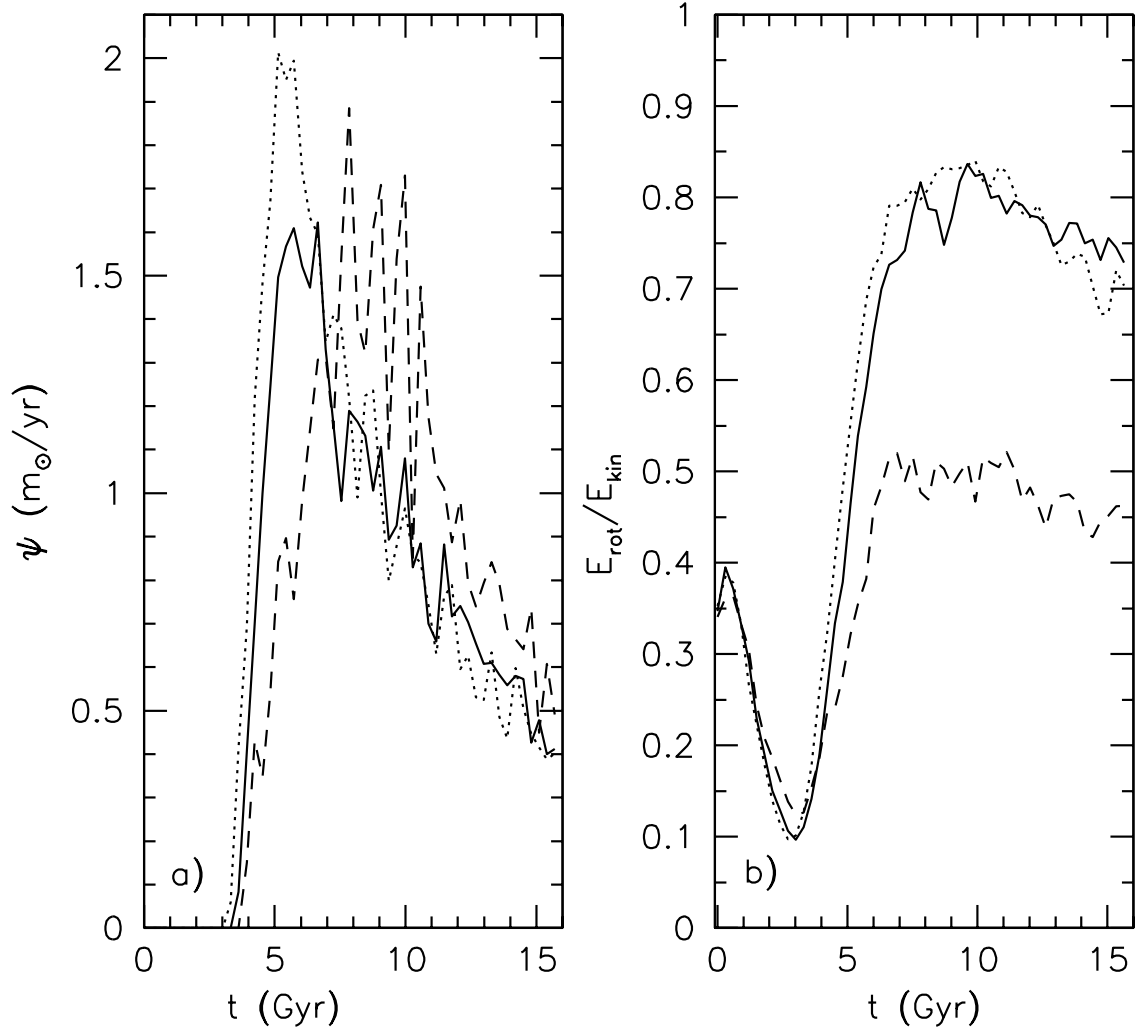


Fig. 6.— Panel a) shows the behavior of the SFR for B3 models with $M_{tot}=20$ and different initial triaxial ratios: continuous line $\tau=0.58$, dotted line $\tau=0.45$ and dashed line $\tau=0.84$; panel b) shows the corresponding rotational support

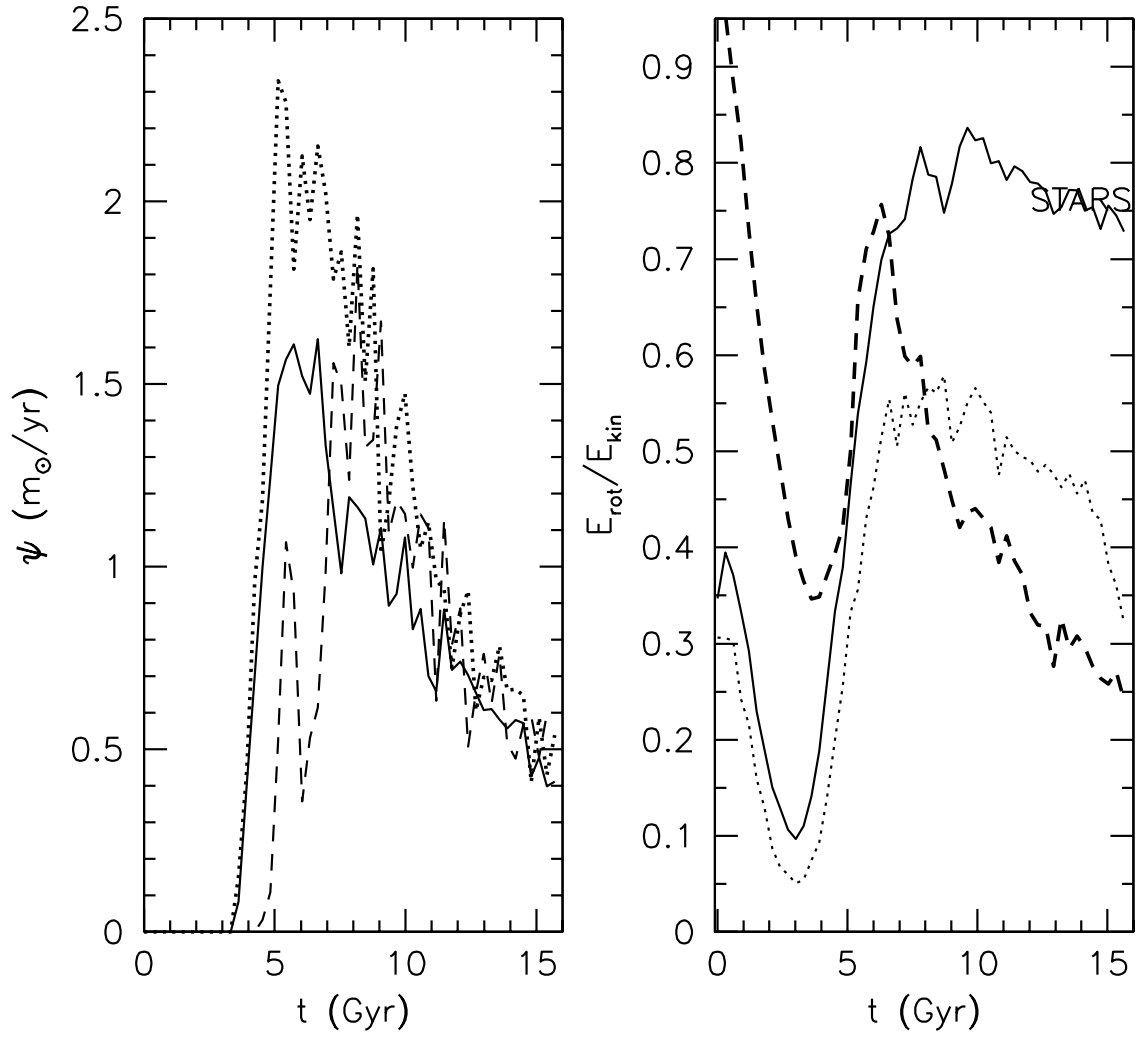


Fig. 7.— As in Fig. 6 but for different initial spin parameters: continuous line $\lambda=0.06$, dotted line $\lambda=0.03$ and dashed line $\lambda=0.15$

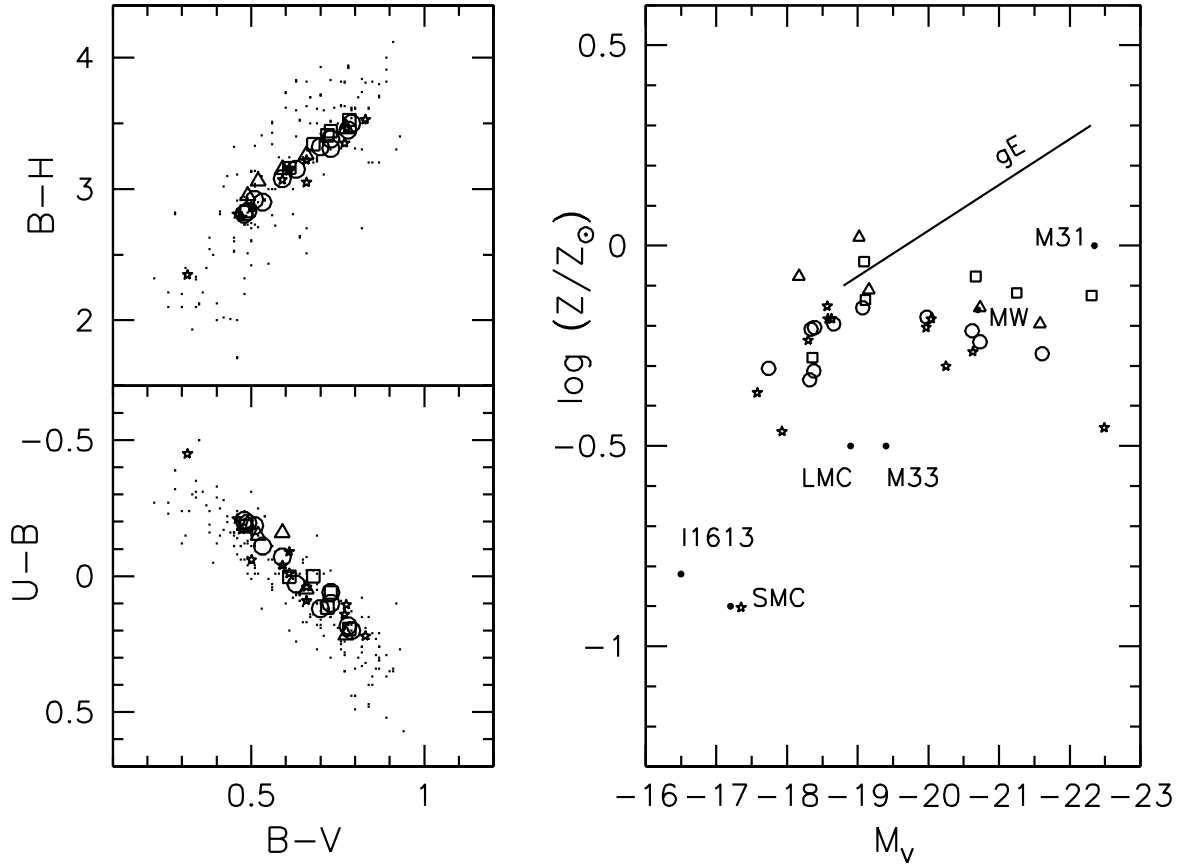


Fig. 8.— Integrated properties at 15 Gyr in the rest-frame of simulations in Table 1: squares are for B1, triangles for B2 and circles for B3 models with $M_{tot}=10, 20, 100, 200$ and 500 (code units) and $M_{bar}/M_{tot}=0.1$; stars are for B3 models with different initial parameters (i.e M_{bar}/M_{tot} , τ and λ values). Dots in the left panels are observations from [50, 51, 52], continuous line and filled circles in the right panel show the metallicity-luminosity relation for giant Ellipticals and for some local systems respectively [53].

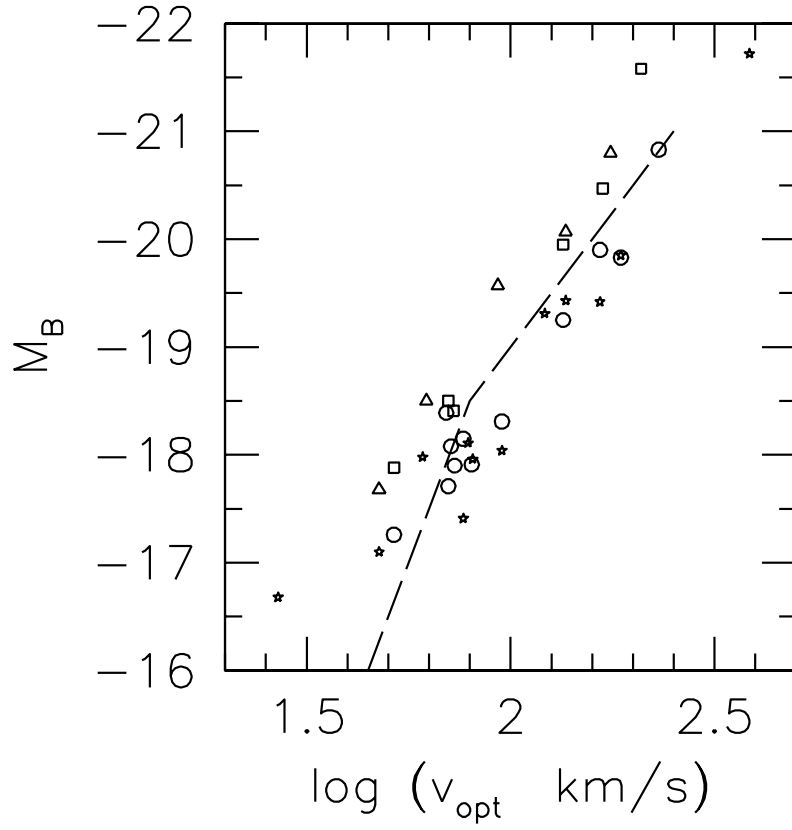


Fig. 9.— B-band TF relation; long-dashed line is the best-fit of the data taken from [54] ($H_0 = 75 \text{ km/s/Mpc}$); v_{opt} is derived from simulations as suggested in [54]; simulations are the same as in Fig. 8.

5. CONCLUSIONS

Our SPH simulations of isolated collapsing triaxial systems with the star formation switched on [4, 6] are aimed to shed light into the dependence of the system evolution on some parameters so far unexplored, as so as its total mass, initial dynamical state and geometrical shape of the DM halo. Further insights into the influence of different values of the baryonic-to-total-mass ratio, M_{bar}/M_{tot} are also given. Important findings are that, for a given value of such a ratio, 0.1 being the fiducial value, the SFR depends on the total mass of the system and on the dynamical state of the halo whose initial geometry affects the results furthermore. These conclusions are not affected by gas particle resolution. Systems with larger M_{tot} turn on the SF earlier on and their SFR achieves higher values than in the less massive halos. Moreover the SF does not switch on in the less massive DM halos so that the critical mass to entail a luminous system is $\simeq 10^{11} m_{\odot}$. According with the time behavior of the rotational support of the baryons, more suitable conditions for elliptical galaxy formation arise in the most massive systems while in the less massive ones, Spirals are favored. Prolate shapes of the collapsing halos, as so as higher spin parameters, delay the onset of the SF process, reduce the star formation activity and provide baryon systems with lower rotational support. Thus, both the star forming activity and the dynamical conditions inside these systems favor Irr or dwarf elliptical galaxy formation. Moreover for a given value of the total mass, that of the DM halo leads the morphological type of the luminous system. In particular, inside the range of parameters explored in paper II, only a short range of values of the baryonic-to-total-mass ratio, around 0.1, is suitable to account for Spirals: the higher the DM mass the lower the rotational support of the baryonic system. Therefore we find that spiral galaxy formation constrains the total mass of the system: $\leq 10^{12} m_{\odot}$. Accounting for the previous conclusions there are no constraints to the total mass of the system hosting an elliptical galaxy. However in the same framework, Ellipticals prefer greater baryonic-to-total-mass ratios as a consequence of both the stronger initial burst of SF which turns on inside them, and the lower rotational support achieved by stars. Moreover our findings shed light into some intriguing point of cosmological simulations of galaxy formation. In particular if feedback effects, in term of both thermal and kinetic energy implementation, can solve the over-cooling problem, a careful baryon's resolution could allow us to overcome the so called "angular momentum crisis" which is, until now, their major challenge.

6. REFERENCES

1. Katz, N., Hernquist, L., and Weinberg, D.H. 1992, ApJ, 399, L109.

2. Barnes, J., and Hernquist, L. 1991, *ApJ* 370, L65.
3. Katz, N., Weinberg, D.H., and Hernquist, L. 1996, *ApJS*, 105, 19.
4. Curir, A., and Mazzei, P. 1999, *New. Astron.* 4, 1; paper I.
5. Springel, V. 2000, *MNRAS*, 312, 859.
6. Mazzei, P., and Curir, A. 2003, *ApJ*, 591, in press; paper II
7. Steinmetz, M., and Navarro, J.F. 2002, *New Astr.* 7, 155.
8. Navarro, J.F., Frenk, C.S., and White, S.D.M. 1996, *ApJ*, 462, 563.
9. Navarro, J.F., Frenk, C.S., and White, S.D.M. 1997, *ApJ*, 490, 493.
10. Moore, B., Governato, F., Quinn, T., Stadel, J., Lake, G. 1998, *ApJ*, 499, 5.
11. Klypin, A., Kravtsov, A.V., Bullock, J.S., and Primack, J.R. 2001, *ApJ*, 554, 903.
12. Steinmetz, M. 2001, *IAU Symp.* 208, 1, Makino, J., Hut, P., eds.
13. Moore, B., Ghigna, S., Governato, F., Lake, G., et al. 1999, *ApJ*, 524, L19.
14. Fukushige, T., and Makino, J. 2001, *ApJ*, 557, 533.
15. Salucci, P., and Burkert, A. 2000, *ApJ*, 537, L9.
16. de Blok, W.J.G., McGaugh, S.S., Bosma, A., and Rubin, V.C. 2001, *ApJ*, 552, L23.
17. de Blok, W.J.G., Bosma, A., and McGaugh, S.S. 2003, *MNRAS*, 340, 657.
18. Huss, A., Jain, B., and Steinmetz, M. 1999, *ApJ*, 517, 64.
19. Klypin, A., Kravtsov, A.V., Valenzuela, O., and Prada, F. 1999, *ApJ*, 552, 82.
20. Steidel, C.C., Adelberger, K.L., Dickinson, M., Giavalisco, M., et al. 1998, *AJ*, 492, 428
21. Navarro, J.F., and Steinmetz, M. 2000, *ApJ*, 538, 477.
22. Ivinson, R., Greve, T., Smail, I., Dunlop, J., and Roche, N. 2002, *MNRAS*, 337, 1
23. Dunne, L., Eales, S., and Edmunds, M.G. 2003, *MNRAS*, 341, 589.
24. Devriendt, J.E.G., and Guiderdoni, B. 2000, *A&A*, 363, 851.
25. White, S.D.M., and Frenk, C.S. 1991, *ApJ*, 379, 52.
26. Kauffmann, G., White, S.D.M., and Guiderdoni, B. 1993, *MNRAS*, 264, 201.
27. Cole, S., Aragon-Salamanca, A., Frenk, C.S., Navarro, J.F., and Zepf, S.E. 1994, *MN-*

- RAS, 271, 781.
28. Cimatti, A., Pozzetti, L., Mignoli, M., et al. 2002, *A&A*, 391, L1.
 29. Kashikawa, N., Takata, T., Ohyama, Y., et al. 2003, *AJ*, 125, 53.
 30. Daddi, E., Broadhurst, T., and Zamorani, G., et al. 2001, *A&A*, 376, 825.
 31. Daddi, E., Cimatti, A., and Broadhurst, T., et al. 2002, *A&A*, 384, L1.
 32. White, S.D.M., and Rees, M.J. 1978, *MNRAS*, 183, 341.
 33. Navarro, J.F., and White, S.D.M. 1994, *MNRAS*, 267, 401.
 34. Kay, S.T., Pearce, F.R., Frenck, C.S., and Jenkins, A. 2002, *MNRAS*, 330, 113.
 35. Katz, N. 1992, *ApJ*, 391, 502.
 36. Steinmetz, M., and Muller, E. 1994, *A&A*, 281, L71.
 37. Navarro, J.F., and White, S.D.M. 1993, *MNRAS*, 265, 271.
 38. Mihos, J.C., and Hernquist, L. 1994, *ApJ*, 437, 611.
 39. Samland, M., and Gerhard, O.E. 2003, *astro-ph/0301499*
 40. Governato, F. Mayer, L., Wadsley, J., et al. 2003, *ApJL* submitted (*astro-ph/0207044*)
 41. Abadi, M.G., Navarro, J.F., and Steinmetz, M. 2003, *ApJ* submitted (*astro-ph/0211331*)
 42. Barnes, J., and Efstathiou, G. 1987, *ApJ*, 319, 575.
 43. Warren, M., S., Quinn, P.J., Salomon, J.K., and Zurek, W.H. 1992, *ApJ*, 399, 405.
 44. Miller, G.E., and Scalo, J.M. 1979, *ApJS*, 41, 513.
 45. Salpeter, E.E. 1955, *ApJ*, 121, 161.
 46. Sandage, A. 1986, *A&A*, 161, 89.
 47. Mazzei, P., Xu, C., and De Zotti, G. 1992, *A&A*, 256, 45.
 48. Mazzei, P., De Zotti, G., and Xu, C. 1994, *ApJ*, 426, 97.
 49. Sackett, P. 1997, *ApJ*, 483, 103.
 50. Bothun D., Aaronson, M., Schommer, B., Mould, B., Huchra, I., and Sullivan, III W., 1985, *ApJS*. 57, 423.
 51. Caldwell, N. 1983, *AJ*, 88, 804.

52. Bothun D., and Caldwell, N. 1984, ApJ, 280, 528.
53. Aaronson, M. 1985, in *Star Forming Dwarf galaxies*, eds. D. Kanth, T.X., Thuan and J., Tran Than Van, p.125.
54. Salucci, P., and Persic, M. 1997, Dark and Luminous Matter in Galaxies, APS Conf. Series, 117, 1.

Table 1. Initial configuration of simulations in paper II.

| N | IMF | N_p | M_{tot} | M_{bar}/M_{tot} | τ | λ |
|----|-----|-------|-----------|-------------------|--------|-----------|
| 1 | B1 | 6000 | 10 | 0.1 | 0.58 | 0.058 |
| 2 | B2 | 6000 | 10 | 0.1 | 0.58 | 0.058 |
| 3 | B3 | 6000 | 10 | 0.1 | 0.58 | 0.058 |
| 4 | B3 | 20000 | 10 | 0.1 | 0.58 | 0.058 |
| 5 | B3 | 6000 | 10 | 0.2 | 0.58 | 0.058 |
| 6 | B3 | 6000 | 10 | 0.99 | 0.58 | 0.058 |
| 7 | B1 | 6000 | 20 | 0.1 | 0.58 | 0.058 |
| 8 | B2 | 6000 | 20 | 0.1 | 0.58 | 0.058 |
| 9 | B3 | 6000 | 20 | 0.1 | 0.58 | 0.058 |
| 10 | B3 | 20000 | 20 | 0.1 | 0.58 | 0.058 |
| 11 | B3 | 6000 | 20 | 0.1 | 0.45 | 0.058 |
| 12 | B3 | 6000 | 20 | 0.1 | 0.84 | 0.058 |
| 13 | B3 | 6000 | 20 | 0.1 | 0.84 | 0.030 |
| 14 | B3 | 6000 | 20 | 0.1 | 0.84 | 0.150 |
| 15 | B3 | 6000 | 20 | 0.05 | 0.58 | 0.058 |
| 16 | B3 | 6000 | 20 | 0.5 | 0.58 | 0.058 |
| 17 | B3 | 6000 | 20 | 0.99 | 0.58 | 0.058 |
| 18 | B1 | 6000 | 100 | 0.1 | 0.58 | 0.058 |
| 19 | B2 | 6000 | 100 | 0.1 | 0.58 | 0.058 |
| 20 | B3 | 6000 | 100 | 0.1 | 0.58 | 0.058 |
| 21 | B3 | 20000 | 100 | 0.1 | 0.58 | 0.058 |
| 22 | B3 | 6000 | 100 | 0.01 | 0.58 | 0.058 |
| 23 | B3 | 6000 | 100 | 0.02 | 0.58 | 0.058 |
| 24 | B3 | 6000 | 100 | 0.99 | 0.58 | 0.058 |
| 25 | B1 | 6000 | 200 | 0.1 | 0.58 | 0.058 |
| 26 | B2 | 6000 | 200 | 0.1 | 0.58 | 0.058 |
| 27 | B3 | 6000 | 200 | 0.1 | 0.58 | 0.058 |

Table 1: continued

| N | IMF | N_p | M_{tot} | M_{bar}/M_{tot} | τ | λ |
|----|-----|-------|-----------|-------------------|--------|-----------|
| 28 | B3 | 20000 | 200 | 0.1 | 0.58 | 0.058 |
| 29 | B3 | 6000 | 200 | 0.1 | 0.45 | 0.058 |
| 30 | B3 | 6000 | 200 | 0.05 | 0.45 | 0.058 |
| 31 | B3 | 6000 | 200 | 0.005 | 0.58 | 0.058 |
| 32 | B3 | 6000 | 200 | 0.010 | 0.58 | 0.058 |
| 33 | B3 | 6000 | 200 | 0.050 | 0.58 | 0.058 |
| 34 | B1 | 6000 | 500 | 0.1 | 0.58 | 0.058 |
| 35 | B2 | 6000 | 500 | 0.1 | 0.58 | 0.058 |
| 36 | B3 | 6000 | 500 | 0.1 | 0.58 | 0.058 |

col.1: simulation number

col.2: see Section 4.1.3

col.3: total number of initial particles

col.4: total mass in unit of $10^{10} m_\odot$

col.5: baryonic-to-total-mass ratio

col.6: initial triaxiality ratio (see Section 4.1.1)

col.7: initial spin parameter (see Section 4.1.1)

Table 2. Properties at 15 Gyr for simulations with $M_{tot} = 20$ and $M_{tot}/M_{bar} = 0.1$ (see text)

| IMF | N_p | r_{eff} | r_D | r_{opt} | $\frac{B}{D}$ | $(\frac{M^*}{L_B})(r_{opt})$ | $(\frac{M^*}{M_{DM}})(r_{opt})$ | f_{gas} |
|-----|-------|-----------|-------|-----------|---------------|------------------------------|---------------------------------|-----------|
| B1 | 6000 | 3.23 | 4.4 | 12.8 | 0.50 | 3.2 | 0.58 | 0.34 |
| B2 | 6000 | 2.78 | 3.5 | 10.5 | 0.70 | 1.9 | 0.49 | 0.62 |
| B3 | 6000 | 4.00 | 4.7 | 13.2 | 0.43 | 7.1 | 0.55 | 0.45 |
| B3 | 2000 | 3.03 | 4.5 | 13.1 | 0.47 | 6.2 | 0.46 | 0.41 |
| B3 | 20000 | 4.18 | 5.0 | 12.8 | 0.44 | 4.9 | 0.42 | 0.58 |
| B3* | 6000 | 2.50 | 7.0 | 17.1 | 1.10 | 16.1 | 0.50 | 0.34 |

* for a model with $f_v=0$

col.1: see Section 4.1.3

col.2: total number of initial particles

col.3: B effective radius (kpc)

col.4: exponential disk scale length (kpc) from B surface brightness distribution

col.5: optical radius (kpc), i.e. radius where $L_B = 0.83L_B^{tot}$ [54]

col.6: bulge-to-disk ratio from $x - y$ projection of B surface brightness distribution

col.7: stellar mass-to B-luminosity ratio inside optical radius

col.8: star-to-DM-mass ratio inside optical radius

col.9: residual gas fraction